Minimum film-boiling quench temperature increase by CuO porous-microstructure coating

Jun-young Kang,[1] Gi Cheol Lee,[2] Massoud Kaviany,[1,3] Hyun Sun Park,[1] Kiyofumi Moriyama,[1] and Moo Hwan Kim[1,a)]
[1]Division of Advanced Nuclear Engineering, POSTECH, Pohang 790-784, South Korea
[2]Department of Mechanical Engineering, POSTECH, Pohang 790-784, South Korea
[3]Department of Mechanical Engineering, University of Michigan, Ann Arbor, Michigan 48109, USA

(Received 19 October 2016; accepted 13 January 2017; published online 24 January 2017)

Increase in the minimum film-boiling quench temperature, T_{MFB}, is achieved with microstructured CuO particles, and attributed to local cooling (fin effect) by the microstructure causing liquid–solid contact. A periodic structure is obtained using electrochemical deposition of 1 μm diameter particles on brass sphere diameter 15 mm forming unit-cell porous cones of average height $L = 100\,\mu$m and base diameter $D = 20\,\mu$m. Fin analysis predicts the cone tip cooling to the homogeneous nucleation temperature of water (~330 °C), while the base temperature is at 600 °C. This causes liquid–solid contact during quenching, and analysis suggests the fin effective thermal conductivity $\langle k \rangle$ and fin characteristic length L^2/D are key to this liquid–solid contact that influences T_{MFB}. *Published by AIP Publishing.* [http://dx.doi.org/10.1063/1.4974923]

The quench-boiling cooling is hindered by the vapor-film insulation in the film-boiling regime,[1] and the minimum film-boiling quench temperature T_{MFB} for stable film is important in sudden cooling of high-temperature systems.[2] The T_{MFB} is strongly influenced by surface conditions including any microstructure,[3–8] such as porous coatings using micron or sub-micron particles,[9–12] and this has been associated with causing liquid–solid contact during boiling.[13] Yet, the role of microstructures in allowing for the liquid–solid contact and the control of structure have not been explored. Control of T_{MFB} is one of the unknowns in boiling phenomena, i.e., "what is the extent and character of liquid-solid contact in film and film-transition boiling?."[14] Strategy to promote the liquid-solid contact by this surface microstructure leads to T_{MFB} increase and contributes to the development of ultra-fast quench system at nuclear power plants, cryogenics, and metallurgy. In this letter, we report on the quench T_{MFB} increase using CuO porous microstructure coating (MPC), and explain the role of the microstructure properties. The electrochemical deposition (ECD) enabled the formation of periodic porous cones with an average particle diameter $d_p = 1\,\mu$m, average height $L = 100\,\mu$m, and base diameter $D = 20\,\mu$m. We explain that quenching results from local cooling, caused by the microstructures, in accordance with the fin theory, and suggest physical parameters controlling the liquid–solid contact.

The quenching experiments are conducted with atmospheric saturated water quenching a sphere (brass, $d_{sphere} = 15$ mm), as shown in Figs. 1(a), and S1 [supplementary material]. The test surfaces were cleaned with acetone, ethanol, and water, and polished with abrasive paper (CW2000-2C; Daesung. We tested three surfaces: the plain surface (PS), and two coated surfaces, the MPC, and a nanostructured coating (NC). The MPC and NC surfaces were fabricated by heat-enhanced ECD which forms CuO particles,[15–17] and the method of Xiao *et al.*[17] [detail in supplementary material S2]. The surface morphology, chemical composition, and surface wettability (contact angle θ_c) were evaluated using field-emission scanning electron microscopy (FE-SEM) with energy dispersive spectrometry (EDS) (JSM7401F; JEOL), X-ray diffraction (XRD) (D/MAX-2500/PC; Rigaku), and a contact angle measurement system (SmartDrop; Femtofab), as shown in Figs. 1(b)–1(f) and supplementary material S3. The MPC surface morphology is formed by interaction between two reaction products ($H_{2(g)}$ and $CuO_{(s)}$) during the ECD process; CuO microparticles cannot uniformly coat the quench sphere surface, due to generation of the H_2 gas and, the CuO microparticles for periodic porous cones. The chemical composition of the MPC and NC was identified as CuO through EDS analysis: Cu(~55%) and O(~45%). The geometric parameters (L and D) in surface structures and θ_c of each test surface are summarized in Table SI (supplementary material S3).

The quench time depends on the surface conditions, and is 57 s for the PS, 50 s for the NC, and 7 s for the MPC, as shown in Fig. 2(a). The temperature history presented as dT/dt before T_{MFB} is characteristic of film-boiling by heat conduction and radiation across the vapor film (8.3 °C/s for PS and NC in the range $400 < T < 550$ °C). The T_{MFB} of NC (300 °C) was higher than that of PS (250 °C), owing to the improvement in surface wettability. However, the MPC surface has a $T_{MFB} > 600$ °C and its large dT/dt (60 °C/s in the range $400 < T < 550$ °C) cannot be explained by vapor conduction film boiling, $q = k_v(T_w - T_{sat})/\delta_v$, where q, k_v, T_w, T_{sat}, and δ_v are the heat flux, vapor thermal conductivity, wall temperature, saturation temperature, and vapor film thickness. This result is consistent with that shown by the high-speed snapshot (Figs. 2(b) and 2(c)) (Multimedia view) captured during the quenching, and the boiling curve (Fig. S4, supplementary material). The liquid–vapor interface was initially perturbed when the PS sphere was immersed in the

a)Author to whom correspondence should be addressed. Electronic mail: mhkim@postech.ac.kr

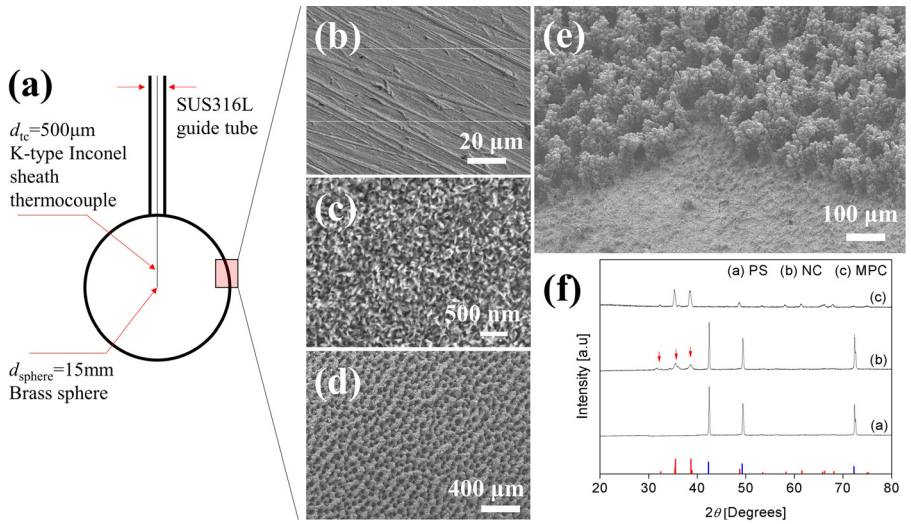

FIG. 1. (a) Quench boiling on metallic sphere, showing thermocouple locations. Surface images by field-emission scanning electron microscopy (FE-SEM) for different surface coatings: (b) plain, (c) nanostructured, and (d), (e) porous microstructures. We used chemical etching (NC sample) and electrochemical deposition (MPC sample) for the surface fabrication in the quench-boiling of metallic sphere, to ensure a complete coating coverage. The coatings fully cover the surface for both samples, and additional FE-SEM images are available in supplementary materials; thickness in NC is below 5 μm (supplementary material, S3). (f) X-ray diffraction patterns in quench samples; the NC have a small peak ascribed to CuO (PDF#48-1548, red line) as well as three large peaks ascribed to GA-Brass (PDF#50-1333, blue line) due to the substrate. In case of MPC, main peak ascribed to CuO is significantly enhanced, indicating a monoclinic crystalline structure. All measurements were conducted under condition: 40 V, 100 mA, $2\theta = 20°$–$80°$ and scan rate = $0.05°$ 2θ s^{-1}.

saturated water, but the stability was recovered, and the film boiling was maintained until the temperature had reached T_{MFB}. The NC sphere behaved in a manner similar to that of the PS, with the collapse of the film occurring quicker than the PS sphere. However, the film boiling on the MPC sphere was unstable, with an explosive evaporation. The liquid–vapor interface was unstable until quenching was complete. This observation implies that the heat transfer mechanism for the MPC differs significantly from the other surface conditions, due to liquid–solid contact throughout quenching.

Several mechanisms cause the liquid–solid contact related to T_{MFB}. First, it has been suggested that the vapor flowing into the porous medium can be absorbed, resulting in T_{MFB} increase.[18] The permeability K of the porous microstructure from the *Carman–Kozeny* relation, $K = \varphi^3 d_p^2/[180(1-\varphi)^2]$, for the MPC sample with porosity $\varphi = 0.5$, and $d_p = 1\,\mu$m gives $K \sim 2.7 \times 10^{-15}$ m^2 (S5, supplementary material), which is too small for a significant permeation. Secondly, the destabilization of the liquid–vapor interface can be attributed to the hydrophilic nature of the metal-oxide microparticles,[19] because a liquid can easily form menisci at the intermittent liquid–solid contact.[20,21] However, an increase in T_{MFB} does not solely result from hydrophilicity, as was demonstrated by the NC surface, which is in agreement with the observations of Kang *et al.*[6] and Fan *et al.*,[22,23] as T_{MFB} increase on superhydrophilic surfaces. Lastly, while a high L/δ_v ratio allows for the liquid–solid contact, it is not a general rule, as reported by Kozlov and Keßler;[7] an increase in T_{MFB} is not solely determined by L/δ_v. Therefore, describing the liquid–solid contact for the MPC sample using the mechanisms discussed above is insufficient. It is known that T_w should be smaller than the homogeneous nucleation temperature, T_{hn}, of water (~330 °C), for maintaining the liquid–solid contact during film boiling,[24] because the liquid phase above T_{hn} must approach the superheat limit. The liquid can make contact the quench surface if it has a local cold region with a temperature that is close to T_{hn}. This is similar to the effects of an insulation layer during quenching.[25,26] Therefore, the temperature gradient of the microstructures needs a close evaluation using the fin theory to determine the possibility of liquid–solid contact.

Considering the liquid–solid contact time $\tau_c \sim 10^{-1}$ s,[27,28] the transient cooling of the microstructures is

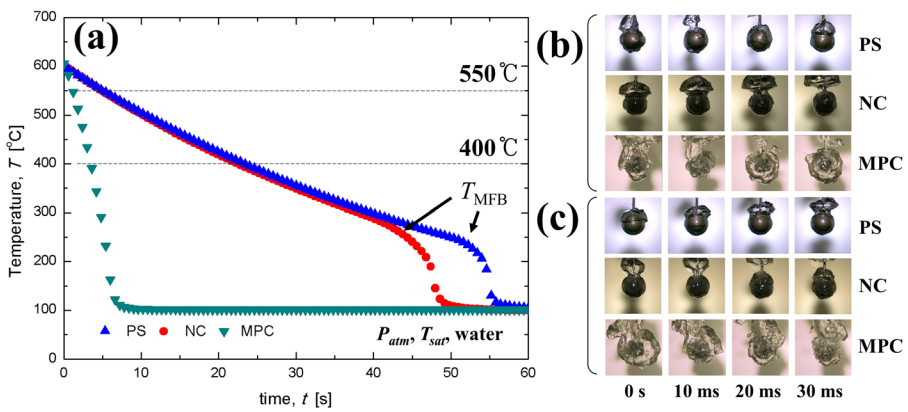

FIG. 2. (a) Quench time is strongly influenced by the surface coating. T_{MFB} is determined by the inflection point of the quench curve. Comparing the plain surface (PS) and nanostructured coating (NC), and explosive evaporation occurs in microstructured-porous coating (MPC): high-speed snapshot at (b) 550 and (c) 400 °C. (Multimedia view) [URL: http://dx.doi.org/10.1063/1.4974923.1] [URL: http://dx.doi.org/10.1063/1.4974923.2] [URL: http://dx.doi.org/10.1063/1.4974923.3]

simplified to quasi-steady state, one-dimensional fin analysis due to a large axial fin Fourier number $Fo_L = \alpha_s \tau_c / L^2$, and small radial fin Biot number $Bi_D = hD/\langle k \rangle$ for the MPC surface ($Fo_L > 1$, and $Bi_D < 10^{-3}$),[29] where α_s, h and $\langle k \rangle$ are the fin thermal diffusivity, heat transfer coefficient, and effective thermal conductivity of microstructures. The fin calculation is based on the *Murray–Gardner assumptions*.[30] The ambient temperature T_{amb} was assumed to be the film temperature $T_f = (T_w + T_{sat})/2$. The geometry of the microstructures is conical spine, as shown in Fig. 3(a), and $\langle k \rangle$ was calculated from the relation $\langle k \rangle = \varphi\, k_v + (1 - \varphi)\, k_{CuO} \cong 0.5$ W/(m K) when $\varphi = 0.5$, $k_v = 0.05$ W/(m K), and thermal conductivity of cupric oxide $k_{CuO} = 1$ W/(m K).[31] The radiation heat flux q_{rad} is negligible in the temperature range $q_{rad} = \sigma_{SB}(T^4 - T_{sat}^4)/[(1/\varepsilon_{CuO}) + (1/\varepsilon_l) - 1] \cong 30\,\text{kW/m}^2$, where the Stefan–Boltzmann constant is $\sigma_{SB} = 5.67 \times 10^{-8}$ W/(m^{-2} K^{-4}), the emissivity of cupric oxide and liquid are $\varepsilon_{CuO} = 1$ and $\varepsilon_l = 1$, and $T = 600\,^\circ$C.[32] The h is calculated using the lumped parameter method, due to the small sphere Biot number; $Bi_{sphere} = hd_{sphere}/k_{sphere} < 0.1$ where d_{sphere} and k_{sphere} are sphere diameter and sphere thermal conductivity (brass), respectively.[33] The temperature difference in microstructures (between fin-tip and fin-base) is strongly dependent on the dimensionless length $mL = [2hL^2/(\langle k \rangle D)]^{1/2}$, i.e.

$$\theta^* = (1/\xi)^{1/2} I_1\left[2^{3/2} m (xL)^{1/2}\right] \Big/ I_1(2^{3/2} mL), \qquad (1)$$

where θ^*, ξ, and I_1 are the dimensionless temperature difference $(T_{x=0} - T_{amb})/(T_{x=L} - T_{amb})$, dimensionless axial position (x/L), and the *modified Bessel function of the first kind of order one*, respectively (supplementary material, S6). $T_{x=0}$ and $T_{x=L}$ are fin-tip and fin-base temperature, respectively. As mL increases, θ^* decreases significantly, as shown in Fig. 3(b). For example, θ^* at $x = 0$ was less than 0.1 for the MPC ($mL \cong 1.3$), and its tip temperature is close to T_{hn} of water. It can be assumed that microstructures at low mL did not cause the local temperature decrease during quenching; θ^* at $x = 0$ is 1 under $mL = 0.06$, where $h = 800$ W/(m^2 K), $L = 100\,\mu$m, $D = 20\,\mu$m, and $k_{brass} = 100$ W/(m K). This result is identical to that of Kim *et al.*[34] the increase in T_{MFB} varies depending

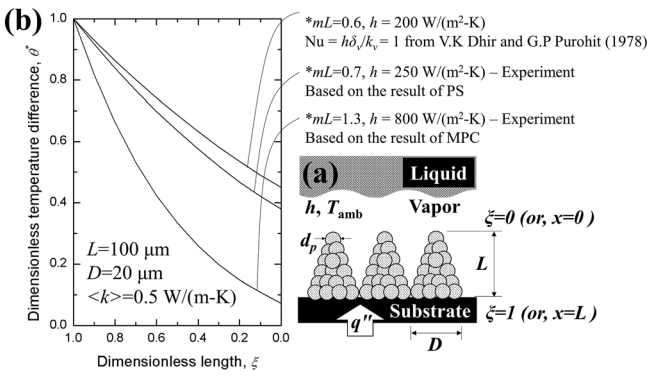

FIG. 3. (a) Schematic of the fin used for thermal analysis (quasi-steady, one dimensional). (b) The temperature profiles with the porous microstructures for different mL, varying h and constant L, D, and $\langle k \rangle$. Temperature at $\xi = 0$ drops to around 350 °C, comparable with $T_{hn} \sim (330\,^\circ$C), while the base temperature is 600 °C. The $mL = 0.6$ is the vapor film thickness $\delta_v = 100\,\mu$m, for comparison with the MPC results.

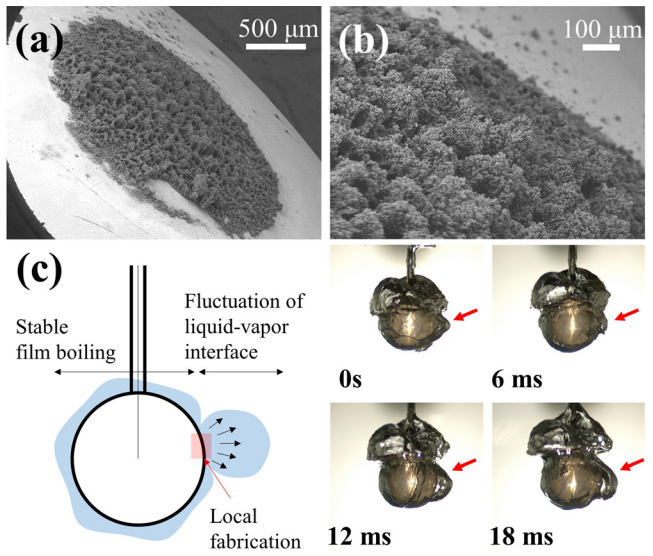

FIG. 4. (a), (b) FE-SEM images of the local spot MPC, and, (c) high-speed snapshots of quench boiling ($T \sim 600\,^\circ$C). The spot area ($A_{coating} = 10^{-6}$ m^2) is small enough to identify the liquid–solid contact during quenching. The liquid-vapor interfacial waves are distinguishable due to the liquid-solid contact on local surface microstructures. The multimedia file provides a clear difference between coated and uncoated part on the quench sphere (supplementary material, S7). (Multimedia view) [URL: http://dx.doi.org/10.1063/1.4974923.4]

on the thermal property of the microstructures (SiO_2, Al_2O_3, and diamond). A low fin efficiency $\eta = 2^{1/2} I_2(2^{3/2} mL)/[mLI_1(2^{3/2} mL)]$ implies that an increase in surface area has little effect on the increase in heat transfer ($\eta < 0.6$ for MPC, and I_2 is the *modified Bessel function of the first kind of order two*). Therefore, porous microstructures can promote liquid–solid contact, even though the quench temperature is 600 °C, and this prevents stable film boiling.

To illustrate the local effect of porous microstructures, note the ratio of the spot area $A_{coating}$ and the total area of the sphere A_{sphere} is about 10^{-3}, as shown in Figs. 4(a) and 4(b). The liquid–solid contact of the microstructures produced liquid–vapor interface with different dynamics (Fig. 4(c)) (multimedia view). The observed variation of the liquid–vapor interface is explained through analysis of the liquid–solid contact, and this phenomena maintains until the quench is over; clear difference in this phenomena is available in supplementary material 7 (image processing conversion). The large mL (through $\langle k \rangle$ and fin characteristic length L^2/D) of CuO porous microstructures improves liquid contact with solid, increasing T_{MFB}. Small $\langle k \rangle$ and large L^2/D cause significant fin tip-cooling, and this is independent of the surface super-hydrophilicity. Microstructures with large mL cause accelerated cooling in high-temperature quenching and the ECD method is promising for such surface modifications.

See supplementary material (S1) for the apparatus of quenching of high temperature sphere, (S2) for coating preparation on quench sphere, (S3) for surface parameters in quench spheres, (S4) for boiling curve, (S5) for vapor absorption in permeable surface, (S6) for fin theory of microstructures, and multimedia video to illustrate the liquid-vapor interface in quench are in (S7).

This work was supported by a National Research Foundation of South Korea (NRF) grant funded by the Korea government (MSIP) (NRF-2015M2A8A2074795). M.K. is grateful for the support by U.S. NSF (Thermal Transport and Processes, CBET16235720).

[1]V. K. Dhir and G. P. Purohit, Nucl. Eng. Des. **47**, 49 (1978).
[2]Y. Y. Hsu, NASA Technical Reports Server Document No. NASA TM X-52837, Lewis Research Center, 1970.
[3]M. Shoji, L. C. Witte, and S. Sankaran, Exp. Therm. Fluid Sci. **3**, 280 (1990).
[4]J. Sinha, Exp. Heat Transfer **16**, 45 (2003).
[5]C. Y. Lee, W. K. In, and Y. H. Koo, J. Nucl. Sci. Technol. **53**, 371 (2015).
[6]J. Kang, S. H. Kim, H. J. Jo, G. Park, H. S. Ahn, K. Moriyama, M. H. Kim, and H. S. Park, Int. J. Heat Mass Transfer **93**, 67 (2016).
[7]N. Kozlov and O. Keßler, Int. J. Heat Thermal Sci. **101**, 133 (2016).
[8]J. Kang, G. C. Lee, M. H. Kim, K. Sridharan, and H. S. Park, in Role of Surface Roughness in Film Boiling Via Saturated Distilled Water Quenching 2016: Proceedings of the 11th International Topical Meeting on Nuclear Reactor Thermal Hydraulics, Operation and Safety, Gyeongju, South Korea, 9–13 October 2016.
[9]J. Y. Chang and S. M. You, Int. J. Heat Mass Transfer **40**, 4437 (1997).
[10]S. G. Liter and M. Kaviany, Int. J. Heat Mass Transfer **44**, 4287 (2001).
[11]H. Kim, J. Kim, and M. H. Kim, Int. J. Heat Mass Transfer **49**, 5070 (2006).
[12]H. S. Ahn and M. H. Kim, J. Heat Transfer **134**, 024001 (2012).
[13]W. S. Bradfield, Ind. Eng. Chem. Fundam. **5**, 200 (1966).
[14]J. H. Lienhard, Int. Commun. Heat Mass Transfer **15.4**, 401–428 (1988).
[15]H. C. Shin and M. Liu, Chem. Mater. **16**, 5460 (2004).
[16]B. J. Plowman, L. A. Jones, and S. K. Bhargava, Chem. Commun. **51**, 4331 (2015).
[17]X. Xiao, L. Miao, G. Xu, L. Lu, Z. Su, N. Wang, and S. Tanemura, Appl. Surf. Sci. **257**, 10729 (2011).
[18]M. Fatehi and M. Kaviany, Int. J. Heat Mass Transfer **33**, 983 (1990).
[19]H. Kim, J. Buongiorno, L. Hu, and T. McKrell, Int. J. Heat Mass Transfer **53**, 1542 (2010).
[20]G. S. Hwang, Y. Nam, E. Fleming, P. Dussinger, Y. S. Ju, and M. Kaviany, Int. J. Heat Mass Transfer **53**, 2662 (2010).
[21]M. A. Hanlon and H. B. Ma, J. Heat Transfer **125**, 644 (2003).
[22]L. Fan, J. Li, D. Li, L. Zhang, and Z. Yu, Int. J. Heat Mass Transfer **76**, 81 (2014).
[23]L. Fan, J. Li, L. Zhang, Z. Yu, and K. Cen, Appl. Therm. Eng. **109**, 630 (2016).
[24]S. Yao and R. E. Henry, J. Heat Transfer **100**, 260 (1978).
[25]F. Moreaux, J. C. Chevrier, and G. Beck, Int. J. Multiphase Flow **2**, 183 (1975).
[26]Y. Kikuchi, T. Hori, and I. Michiyoshi, Int. J. Heat Mass Transfer **28**, 1105 (1985).
[27]L. Lee and J. C. Chen, Rev. Sci. Instrum. **53**, 1472 (1982).
[28]Y. Kikuchi, T. Ebisu, and I. Michiyoshi, Int. J. Heat Mass Transfer **35**, 1589 (1992).
[29]J. H. Lienhard, *A Heat Transfer Textbook*, 3rd ed. (Phlogiston Press, Cambridge, 2008), p. 163.
[30]A. D. Kraus, A. Aziz, and J. Welty, *Extended Surface Heat Transfer* (John Wiley & Sons, Inc., NY, 2001), p. 10.
[31]G. V. Samsonov, *The Oxide Handbook* (IFI/Plenum Data Corporation, NY, 1973), p. 115.
[32]E. M. Sparrow, Int. J. Heat Mass Transfer **7**, 229 (1964).
[33]F. P. Incropera, D. P. Dewitt, T. L. Bergman, and A. S. Lavine, *Fundamentals of Heat and Mass Transfer*, 6th ed. (John Wiley & Sons, Inc., NY, 2007), p. 261.
[34]H. Kim, G. DeWitt, T. McKrell, J. Buongiorno, and L. Hu, Int. J. Multiphase Flow **35**, 427 (2009).